Measurement and Modeling of Magnetomechanical Coupling in Magnetostrictive Iron-Gallium Alloys

Phillip G. Evans, Marcelo J. Dapino

The Ohio State University, 201 W 19th Ave, Columbus, OH 43210 USA

ABSTRACT

Measurements are performed to characterize the nonlinear and hysteretic magnetomechanical coupling of iron-gallium (Galfenol) alloys. Magnetization of production and research grade Galfenol is measured under applied stress at constant field, applied field at constant stress, and alternately applied field and stress. A high degree of reversibility in the magnetomechanical coupling is observed by comparing a series of applied field at constant stress experiments with a single applied stress at constant field experiment. Accommodation is not evident and magnetic hysteresis for both applied field and stress is shown to be coupled. A stress, field, and orientation dependent hysteron is developed from continuum thermodynamics which employs a unified hysteresis mechanism for both applied stress and field. The hysteron has an instantaneous loss mechanism similar to Coulomb-friction or Preisach-type models and is shown to satisfy the second law of thermodynamics. Stochastic homogenization is employed to account for the smoothing effect that material inhomogeneities have on the magnetization.

1. INTRODUCTION

Magnetostrictive materials exhibit dimensional changes in response to magnetic fields and change magnetic state in response to applied stress. These effects have been used to create actuators and sensors which deliver superior performance with less weight, size and moving parts than traditional electromagnetic devices. Iron-gallium alloys (Galfenol) with 12-19 atomic percent gallium are a new class of magnetostrictive materials which have both high magnetically induced strain or magnetostriction ($\sim$400 ppm) and steel-like structural properties [1]. Prior to the advent of Galfenol, magnetostrictive materials included mechanically robust materials with low magnetostriction such as iron and nickel and brittle materials with giant magnetostriction such as Terfenol-D (Fe-Tb-Dy.) This unique combination of mechanical robustness and high magnetostriction makes Galfenol ideal for creating sensors and actuators that can take tension, bending and torsion and shock loads in harsh environments. Furthermore, Galfenol can be machined, welded, extruded, and deposited into complex geometries.

While linear characterization of Galfenol has been performed [2, 3], a nonlinear description of the magnetomechanical behavior including hysteresis has not been done. In this work, magnetization measurements of production and research grade Galfenol from Etrema Products, Inc. are presented. Experiments include applied magnetic field at constant stress, applied stress at constant field, and alternately applied field and stress. The measurements show a remarkable degree of reversibility in the magnetomechanical coupling, even in the production grade sample, which is in contrast with the magnetomechanical coupling in steel [4, 5]. This is evidenced by comparing the magnetization versus stress curve generated by varying the stress at a constant bias field and the same curve generated by varying the field at different bias stresses and selecting the magnetization at the chosen bias field. The two curves are nearly identical. Accommodation is not evident in minor loops consisting of decreasing the field from a bias point, decreasing stress from a bias point, returning the field, and returning the stress. Repeated field and stress cycles overlap. These measurements indicate that the same loss mechanism causes magnetic hysteresis for both applied stress and applied magnetic field.

A hysteron is developed from continuum thermodynamics which employs a unified loss mechanism for magnetic hysteresis under both applied field and stress. In contrast with the Preisach model which uses a hysteron with constant magnetic states, the states developed here are magnetic field and stress dependent. Magnetic field and stress cause 3-D rotations of domains about the easy crystal directions. These rotations are calculated from energy principles and are the hysteron states. The number of hysteron states is thus dictated by material symmetry and anisotropy which determine the easy directions. Magnetic field and stress also causes switching between energy states when the energy difference between the current state and the global minimum reaches a critical level.

Behavior and Mechanics of Multifunctional Materials and Composites 2009, edited by Zoubeida Ounaies, Jiangyu Li,
Proc. of SPIE Vol. 7289, 72891X · © 2009 SPIE · CCC code: 0277-786X/09/$18 · doi: 10.1117/12.815826

The effect of material impurities and defects is accounted for through stochastic homogenization. Following the approach of Smith et al. [6, 7], a statistically distributed interaction field is superimposed on the applied field. Rather than employ a 3-D, statistically distributed coercive field, a scalar coercive energy is used in the homogenization scheme resulting in fewer computations. This model enables the design and control of smart structures with 3-D multi-functionality that take advantage of the full nonlinear range of magnetomechanical coupling of Galfenol.

2. MEASUREMENTS

Measurements are performed at the Naval Surface Warfare Center, Carderock Division on $\langle 100 \rangle$ oriented, production and research grade Galfenol samples from Etrema Products, Inc. in rod form with dimensions of 0.25×1 inches. Stress is applied with an MTS 858 tabletop system, capable of applying compressive loads only, by loading the sample between parallel plates. Magnetic field is applied with a drive coil situated with the Galfenol sample in a steel canister providing a flux return path. Since the permeability of Galfenol is similar to that of the steel return path, it is necessary to use a feedback controller for the magnetic field. The changing permeability of Galfenol results in a nonlinear relationship between the voltage applied to the drive coil and the magnetic field in the Galfenol sample. Drive coil voltage is supplied by a Test Star II MTS controller. The level of voltage required to achieve a desired reference field is found by measuring the field with a Lakeshore 421 gauss meter and implementing a PI controller with an NI SCB-69 DAQ acquisition board. Magnetic flux density is measured with a Walker Scientific MF-30 fluxmeter and pick-up coil. Magnetization is calculated by subtracting the field measurements from flux density measurements.

2.1. Production Grade 18.4 at% Ga

Major magnetization loops for applied magnetic field at constant stress and applied stress at constant field are shown in Figure 1. Magnetization versus field measurements have two regions of noticeable hysteresis, one at low fields and another at higher fields. Consider for example the curve obtained under 79 MPa compressive stress. There is a hysteretic region below 1 kA/m and another between 7-12 kA/m. The higher field region moves higher with increasing stress. Details of how these regions arise from anisotropy and magnetomechanical coupling are discussed in Section 3. The magnetization versus stress, at low stresses, depends strongly on the field history. The curves in Figure 1(b) are measured after applying a positive saturating field and subsequently lowering the field to the bias point while the curves in Figure 1(c) are measured after applying a negative saturating field and subsequently bringing the field to the bias point. In the latter, multiple loops overlap while in the former, the first loop does not close. An exception is the case where there is zero bias field after having negatively saturated the material. In this case the negative remanence resulting from bringing the field from negative saturation to zero, is wiped out by the stress. Further cycles of the stress do not result in any magnetization change. This is interpreted in Section 3 as the result of differing initial domain orientations.

Measurements shown in Figure 2 show a remarkable degree of reversibility in the magnetomechanical coupling of Galfenol. In 2(a) a magnetization versus stress curve at constant field is obtained from direct measurement and compared to magnetization versus stress points obtained from multiple sets of magnetization versus field measurements at different bias stress levels. The points are obtained from the upper and lower branches of the magnetization versus field hysteresis curves at the bias field level. These points are then plotted versus the respective bias stresses at which the magnetization versus field curves are measured. The overlap of the curve measured directly while applying stress and the points obtained from magnetization versus field curves at constant stress suggests that the magnetomechanical coupling is reversible and magnetization hysteresis from applied field and applied stress results from the same physical mechanism.

Figure 2(b) shows measurements from alternately applied field and stress along with two magnetization versus stress curves at constant field. The two magnetization versus stress curves are obtained by first positively saturating the material and lowering the field to the bias point. A stress is then cycled three times to -70 MPa. As before, the first loop is not closed. The curve from alternate stress and field application is initialized in the same manner by saturating positive and lowering the field to the first bias field of 2.8 kA/m. Thus as stress is applied it follows the magnetization versus stress curve with the higher bias field. At 12.6 MPa compression the stress is held constant and the field is lowered to 2 kA/m from its previous 2.8 kA/m. This moves the

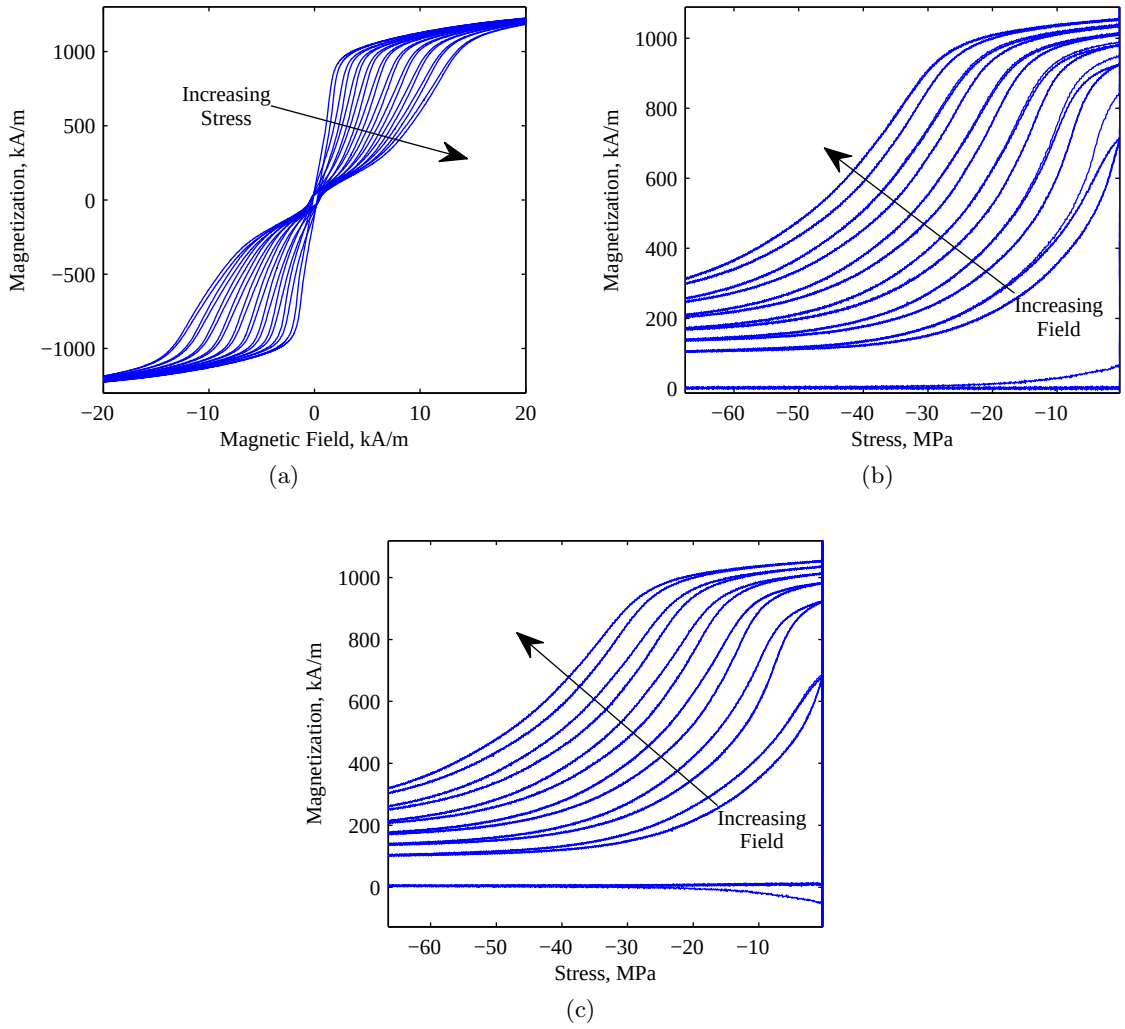

Figure 1. Major magnetization loops of production grade Fe-Ga from (a) applied field with constant stress levels of 0, −11, −19, −26, −35, −44, −52, −61, −70, −79 MPa and (b),(c) applied stress with constant field levels of 0, 1.6, 2.4, 3.3, 4.0, 4.8, 5.6 kA/m with (b) saturated positive and (c) saturated negative before bias field application.

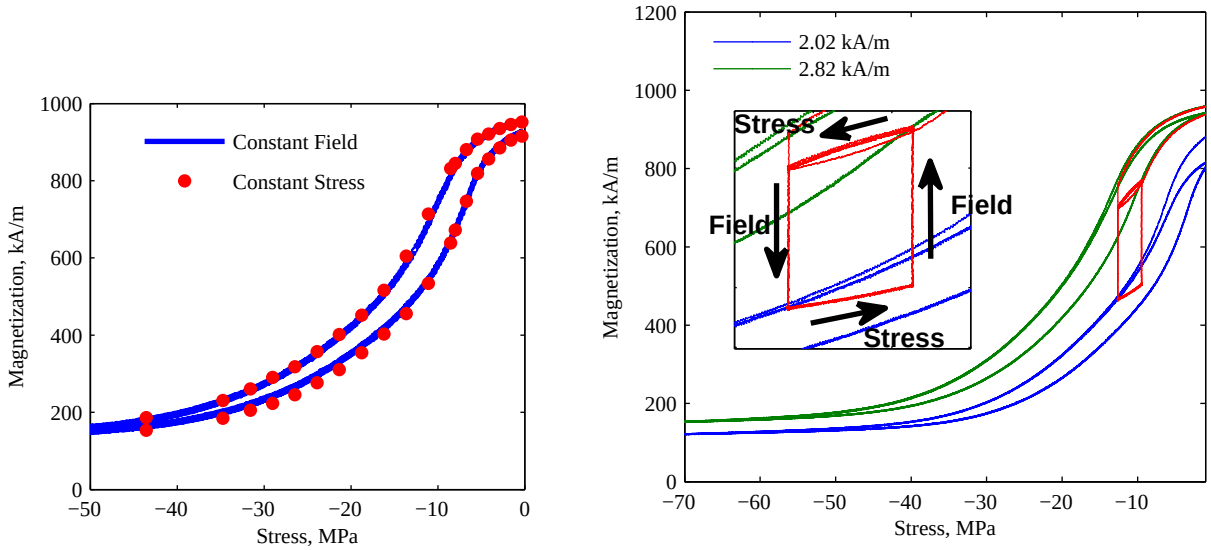

(a) (b)

Figure 2. (a) Comparison of production grade Fe-Ga magnetization versus stress at 2.8 kA/m field obtained from sensing and actuation measurements and (b) minor loops from alternately varying the field between 2 and 2.8 kA/m and the stress between 9.4 and 12.6 MPa compression, with the cycle repeated three times.

magnetization from the upper branch of the magnetization versus stress curve at the higher bias field to the upper branch of the magnetization versus stress curve at the lower bias. Here the field is again held constant and the stress is relaxed to 9.4 kA/m resulting in a shift of the magnetization towards the lower branch of major magnetization versus stress loop. The stress is again held constant and the field is returned to 2.8 kA/m bringing the magnetization to the lower branch of the magnetization versus stress curve obtained with a 2.8 kA/m bias field. The stress is then returned to 12.6 MPa at constant field, moving the magnetization towards the upper branch of the magnetization versus stress major loop. This stress and field cycle is repeated three times before returning the stress to zero. These minor loops obtained by alternately applying field and stress about a bias point lack any noticeable accommodation. This is in contrast with measurements of steel which exhibit large changes in the shape of magnetization loops obtained from cycling the stress and field [4, 5].

2.2. Research Grade 18.5 at% Ga

Major magnetization loops of research grade material have similarities with the production grade material. Specifically, the field location of the burst region is moved to higher fields with increasing bias stress (see Figure 3(a).) The loops however do not have a noticeable hysteretic region at low fields as do the production grade magnetization loops. This will be shown to result from an improved alignment of the crystal lattice with the rod axis. Additionally, the nonlinear susceptibility is higher in the research grade samples. The magnetization versus stress loops (see Figure 3(b)) are similar to the production grade measurements where the first cycle is not closed and subsequent cycles overlap. They differ in the high slope regions, having mush sharper transitions. This is attributed to the research grade material having fewer material imperfections. The magnetomechanical coupling in the research grade material is also seen to be reversible by comparing the magnetization versus stress measured at constant field and the magnetization versus stress measured at constant stress in the same manner as was done with the production grade material (see Figure 4(a).)

The coupled nature of the hysteresis mechanism observed in the magnetization from both applied field and applied stress is emphasized in Figure 4(b). Starting from a field of 4.2 kA/m and compressive stress of 15 MPa, if the magnetization starts at point A on the upper branch of the major magnetization versus field loop, increasing the stress and returning to 15 MPa pushes the magnetization to point B on the lower branch of the major loop

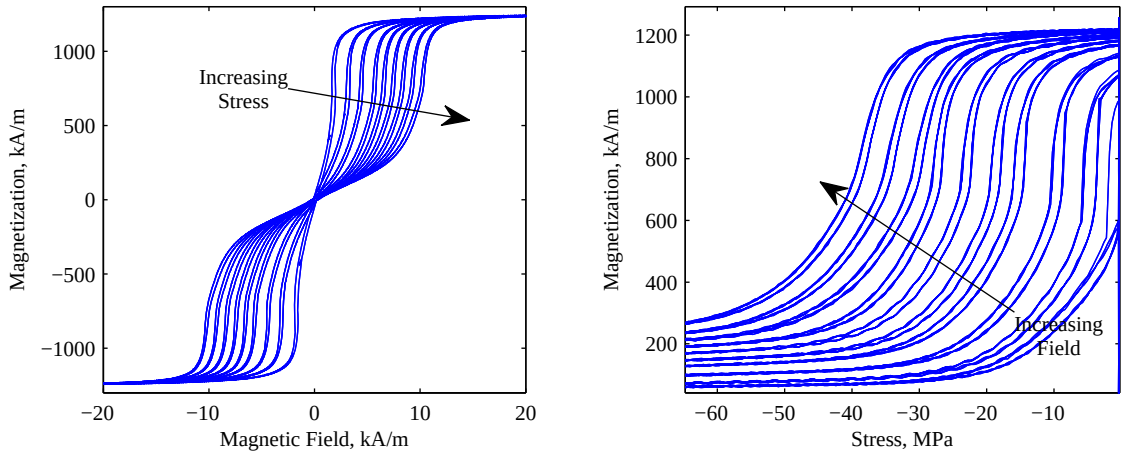

(a) (b)

Figure 3. Major magnetization loops of research grade Fe-Ga from (a) applied field with constant stress levels of 0, −9, −16, −23, −28, −32, −37, −42, −46 MPa and (b) applied stress with constant field levels of 1.9, 4.2, 2.4, 3.2, 4.8, 5.6, 6.5, 7.3, 8.1, 8.9 kA/m.

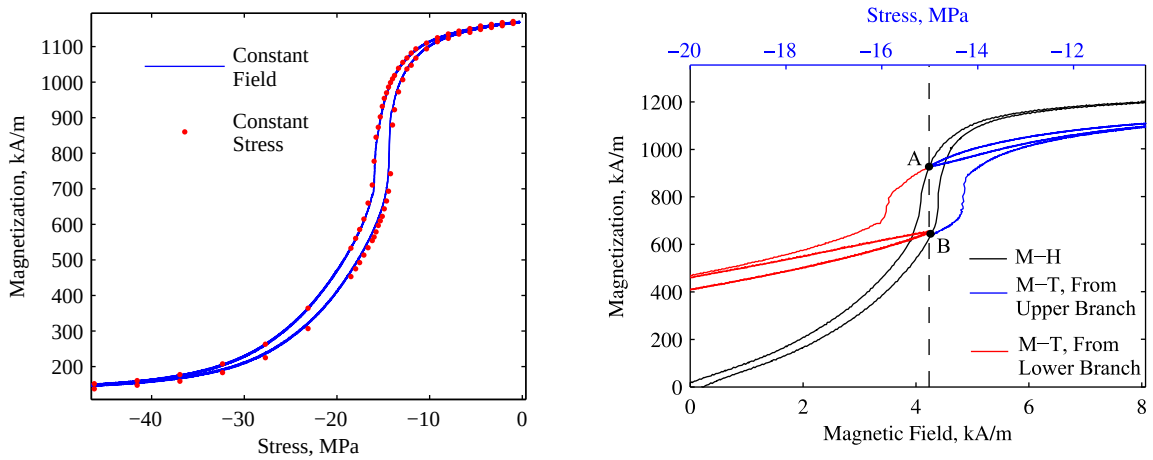

(a) (b)

Figure 4. (a) Comparison of research grade Fe-Ga magnetization versus stress at 4.2 kA/m field obtained from sensing and actuation measurements and (b) magnetization excursions from the upper and lower hysteresis branches about a bias of 15 MPa and 4.2 kA/m, cycled three times.

in a single cycle. Further cycles always return to point B on the lower branch and overlap. Starting at point B on the lower branch of the hysteresis loop, when the stress is lowered to zero and brought back to 15 MPa, the magnetization is pushed to point A on the upper branch of the major loop. Further cycles always return to the upper branch of the major loop and overlap. These results show that the width of the hysteresis loops for applied stress and applied field are constrained in that knowledge of one determines the other.

3. MODEL DEVELOPMENT

A constitutive model relating magnetization and strain to magnetic field and stress will be developed from thermodynamic principles with stochastic homogenization. A hysteron for single crystal material devoid of imperfections is first derived from thermodynamic principles. Stochastic homogenization is then employed to incorporate the smoothing effect of material inhomogeneities.

The first law of thermodynamics states that the rate of change of the internal energy U is equal to the rate of change of the applied work plus generated heat, less the heat leaving. For a thermo-magneto-mechanical material with stress $\mathbf{T}$ and strain $\mathbf{S}$ (using vector notation), magnetic field $\mathbf{H}$, magnetization $\mathbf{M}$, heat generation Q and heat flux $\mathbf{q}$, this is expressed by

$$\dot{U} = \mathbf{T} \cdot \dot{\mathbf{S}} + \mu_0 \mathbf{H} \cdot \dot{\mathbf{M}} + Q - \nabla \cdot \mathbf{q}. \tag{1}$$

The second law of thermodynamics states that thermal processes result in entropy η increase. At temperature θ this can be expressed through the Clausius-Duhem inequality

$$\dot{\eta} \geq \frac{Q}{\theta} - \nabla \cdot \left(\frac{\mathbf{q}}{\theta} \right). \tag{2}$$

Eliminating the heat generation by combining the first and second laws gives

$$\theta \dot{\eta} - \dot{U} + \mathbf{T} \cdot \dot{\mathbf{S}} + \mu_0 \mathbf{H} \cdot \dot{\mathbf{M}} - \frac{1}{\theta} \mathbf{q} \cdot \nabla \theta \geq 0. \tag{3}$$

The dependencies are

$$U = U(\mathbf{S}, \mathbf{M}, \eta), \tag{4}$$
$$\mathbf{T} = \mathbf{T}(\mathbf{S}, \mathbf{M}, \eta), \tag{5}$$
$$\mathbf{H} = \mathbf{H}(\mathbf{S}, \mathbf{M}, \eta). \tag{6}$$

In practice it is easier measure magnetization and strain as a function of field, stress, and temperature. Furthermore, the magnetization can be interpreted as being a function of internal variables representing r possible domain orientations $\mathbf{m}^k$ and domain volume fractions ξ^k. The internal variables will provide a mechanism for energy dissipation leading to a unified hysteresis mechanism for both applied field and stress. The dependencies are switched through the Legendre transformation

$$G(\mathbf{H}, \mathbf{T}, \theta) = U(\mathbf{M}, \mathbf{S}, \eta) - \eta\theta - \mathbf{S} \cdot \mathbf{T} - \mu_0 \mathbf{M} \cdot \mathbf{H}. \tag{7}$$

Since magnetization is also dependent on the internal variables $\mathbf{m}^k$ and ξ^k, the dependencies after transformation are

$$\mathbf{M} = \mathbf{M}(\mathbf{H}, \mathbf{T}, \theta, \mathbf{m}^k, \xi^k), \tag{8}$$
$$\mathbf{S} = \mathbf{S}(\mathbf{H}, \mathbf{T}, \theta, \mathbf{m}^k, \xi^k), \tag{9}$$
$$\eta = \eta(\mathbf{H}, \mathbf{T}, \theta, \mathbf{m}^k, \xi^k). \tag{10}$$

The time rate of change of the free energy G is then

$$\dot{G} = \frac{\partial G}{\partial \mathbf{H}} \cdot \dot{\mathbf{H}} + \frac{\partial G}{\partial \mathbf{T}} \cdot \dot{\mathbf{T}} + \frac{\partial G}{\partial \theta} \dot{\theta} + \sum_{k=1}^{r} \left[\frac{\partial G}{\partial \mathbf{m}^k} \cdot \dot{\mathbf{m}}^k + \frac{\partial G}{\partial \xi^k} \dot{\xi}^k \right]. \tag{11}$$

From (7), the time rate of change of the internal energy is

$$\dot{U} = \dot{G} + \eta\dot{\theta} + \theta\dot{\eta} + \mathbf{S}\cdot\dot{\mathbf{T}} + \mathbf{T}\cdot\dot{\mathbf{S}} + \mu_0\mathbf{H}\cdot\dot{\mathbf{M}} + \mu_0\mathbf{M}\cdot\dot{\mathbf{H}}. \tag{12}$$

Substitution of (12) and (11) into (3) gives

$$-\left(\eta + \frac{\partial G}{\partial\theta}\right)\dot{\theta} - \left(\mu_0\mathbf{M} + \frac{\partial G}{\partial\mathbf{H}}\right)\dot{\mathbf{H}} - \left(\mathbf{S} + \frac{\partial G}{\partial\mathbf{T}}\right)\dot{\mathbf{T}} + \sum_{k=1}^{r}\left[\frac{\partial G}{\partial\mathbf{m}^k}\cdot\dot{\mathbf{m}}^k + \frac{\partial G}{\partial\xi^k}\dot{\xi}^k\right] - \frac{1}{\theta}\mathbf{q}\cdot\nabla\theta \geq 0. \tag{13}$$

For thermo-magneto-mechanical materials that are reversible, the inequality becomes an equality and the constitutive relations can be found from

$$\mu_0\mathbf{M} = -\frac{\partial G}{\partial\mathbf{H}}, \tag{14}$$

$$\mathbf{S} = -\frac{\partial G}{\partial\mathbf{T}}, \tag{15}$$

$$\eta = -\frac{\partial G}{\partial\theta}, \tag{16}$$

$$\frac{\partial G}{\partial\xi_k} = 0, \tag{17}$$

$$\frac{\partial G}{\partial\mathbf{m}^k} = 0, \tag{18}$$

$$\mathbf{q} = -k\nabla\theta. \tag{19}$$

Now the following assumptions are made on the processes

- Isothermal
- Negligible temperature gradients
- Reversible domain rotation
- Irreversible domain volume fraction evolution

With these assumptions, the following constitutive relationships are consistent with the first and second laws of thermodynamics

$$\mu_0\mathbf{M} = -\frac{\partial G}{\partial\mathbf{H}}, \tag{20}$$

$$\mathbf{S} = -\frac{\partial G}{\partial\mathbf{T}}, \tag{21}$$

$$\frac{\partial G}{\partial\mathbf{m}^k} = 0, \tag{22}$$

$$-\frac{\partial G}{\partial\xi_k}\dot{\xi}^k \geq 0. \tag{23}$$

For this case, dissipation occurs as domains reconfigure. The free energy and volume fraction evolutions need to be defined. The energy has terms for magnetic anisotropy G_A, magnetomechanical coupling G_C, Zeeman or field energy G_Z, and elastic strain energy G_E. These energies will be expressed while idealizing the complex domain structure of ferromagnetic materials as a system of non-interacting, single-domain, Stoner-Wohlfarth (S-W) particles. For anisotropic, ferromagnetic materials having r preferred or easy domain orientations $\mathbf{c}^r$, the anisotropy energy is the work required to rotate a S-W particle away from its easy direction. This is analogous to mechanical systems where work is required to displace a spring from equilibrium. The anisotropy energy of a single S-W particle with easy direction $\mathbf{c}^k$ is

$$G_A^k = \frac{1}{2}K^k(\theta)|\mathbf{m}^k - \mathbf{c}^k|^2. \tag{24}$$

For cubic materials, the $\langle 100\rangle$ or $\langle 111\rangle$ tend to be the easy directions. The anisotropy coefficient in each direction family is the same, thus $K^k = K_{100}$ for all six $\langle 100\rangle$ directions and $K^k = K_{111}$ for all eight $\langle 111\rangle$ directions. For negative anisotropy coefficients K^k, the direction $\mathbf{c}^k$ is magnetically hard or an unstable equilibrium. For the isothermal processes considered here the anisotropy coefficients are constant. The magnetomechanical energy for a S-W single particle is the strain energy density resulting from its magnetostriction $\boldsymbol{\lambda}^k$

$$G_C^k = -\boldsymbol{\lambda}^k \cdot \mathbf{T}, \tag{25}$$

and its Zeeman energy is

$$G_Z^k = -\mu_0 M_s(\theta)\mathbf{m} \cdot \mathbf{H}, \tag{26}$$

where M_s is the magnetization of a S-W particle, constant for isothermal processes. The magnetostriction of a S-W particle for cubic materials is [8]

$$\boldsymbol{\lambda}^k = \begin{bmatrix} (3/2)\lambda_{100}\left(m_1^k\right)^2 \\ (3/2)\lambda_{100}\left(m_2^k\right)^2 \\ (3/2)\lambda_{100}\left(m_3^k\right)^2 \\ 3\lambda_{111}m_1^k m_2^k \\ 3\lambda_{111}m_2^k m_3^k \\ 3\lambda_{111}m_3^k m_1^k \end{bmatrix}. \tag{27}$$

The mechanical strain energy of the material is

$$G_E = -\frac{1}{2}\mathbf{T} \cdot \mathbf{s}\mathbf{T}, \tag{28}$$

where the 6×6 compliance $\mathbf{s}$ has symmetry consistent with the material crystal structure. Summing the energy terms and weighting with the volume fractions, the free energy of the material is

$$G = \sum_{k=1}^{r} \xi^k G^k + \mathbf{T} \cdot \mathbf{s}\mathbf{T}, \tag{29}$$

$$G^k = K^k|\mathbf{m}^k - \mathbf{c}^k|^2 - \boldsymbol{\lambda}^k \cdot \mathbf{T} - \mu_0 M_s \mathbf{m}^k \cdot \mathbf{H}. \tag{30}$$

From (20), the magnetization is

$$\mathbf{M} = -\frac{1}{\mu_0}\frac{\partial G}{\partial \mathbf{H}} = M_s \sum_{k=1}^{r} \xi^k \mathbf{m}^k, \tag{31}$$

and the strain is

$$\mathbf{S} = -\frac{\partial G}{\partial \mathbf{T}} = \sum_{k=1}^{r} \xi^k \boldsymbol{\lambda}^k + \mathbf{s}\mathbf{T}. \tag{32}$$

3.1. Calculation of particle orientations

The magnetic orientations $\mathbf{m}^k$ of the S-W particles are calculated from the minimization (22). This minimization is constrained since the vector $\mathbf{m}^k$ is a unit vector. The constraint is $C = |\mathbf{m}^k| - 1 = 0$. The constrained minimization can be cast in the form of an inhomogeneous eigenvalue problem by using Lagrange multipliers. Gathering terms from (30) and expressing the particle free energy as $G^k = \frac{1}{2}\mathbf{m}^k \cdot \mathbf{K}^k\mathbf{m}^k - \mathbf{m}^k \cdot \mathbf{B}^k$ the eigenvalue problem is

$$\left(\mathbf{K}^k - \alpha\mathbf{I}\right)\mathbf{m}^k = \mathbf{B}^k, \tag{33}$$

where the magnetic stiffness matrix $\mathbf{K}^k$ and force vector $\mathbf{B}^k$ are

$$\mathbf{K}^k = \begin{bmatrix} K^k - 3\lambda_{100}T_1 & -3\lambda_{111}T_4 & -3\lambda_{111}T_6 \\ -3\lambda_{111}T_4 & K^k - 3\lambda_{100}T_2 & -3\lambda_{111}T_5 \\ -3\lambda_{111}T_6 & \lambda_{111}T_5 & K^k - 3\lambda_{100}T_3 \end{bmatrix}, \tag{34}$$

$$\mathbf{B}^k = \begin{bmatrix} c_1^k K^k + \mu_0 M_s H_1 & c_2^k K^k + \mu_0 M_s H_2 & c_3^k K^k + \mu_0 M_s H_2 \end{bmatrix}^{\mathrm{T}}. \tag{35}$$

While the orientation can be easily solved for in terms of α through diagonalization, determination of α requires solution of a six order polynomial obtained by substituting the α dependent orientation into the constraint. The constraint is relaxed through linearization about the easy direction $\mathbf{c}^k$. This is accurate because as a field or stress pulls a particle away from the easy direction, at a critical energy level the particle flips to an equilibrium closer to the applied field or perpendicular to the applied principal stresses. This is modeled through an instantaneous change in the volume fractions ξ^k. For the relaxed, linear constraint, the solution to the inhomogeneous eigenvalue problem is

$$\mathbf{m}^k = \left(\mathbf{K}^k\right)^{-1} \left[\mathbf{B}^k + \frac{1 - \mathbf{c}^k \cdot \left(\mathbf{K}^k\right)^{-1} \mathbf{B}^k}{\mathbf{c}^k \cdot \left(\mathbf{K}^k\right)^{-1} \mathbf{c}^k} \mathbf{c}^k\right]. \tag{36}$$

The reduction in computational expense by relaxing the constraint is beneficial for the stochastic homogenization which will be employed. The particle orientations (36) define the possible states of a 3D, anisotropic, field and stress dependent magnetization and strain hysteron at the particle level. The magnetization of the hysteron is calculated from (31) and the strain from (32). An evolution equation for the volume fractions ξ^k will be defined in the next section. This evolution defines the switches in the hysteron states and is consistent with the second law of thermodynamics. Finally, certain parameters in the hysteron are assumed to be manifestations of underlying distributions and the bulk material magnetization and strain is calculated through stochastic homogenization.

3.2. Evolution of domain volume fractions and hysteron construction

A model is proposed for the evolution of the volume fractions ξ^k which satisfies (23). The Preisach model has been used successfully for hysteretic materials and can be physically interpreted as a summation of magnetization hysterons which have delayed, instantaneous switches in the magnetization state due to a Coulomb-friction type loss. A similar approach is taken here.

At the domain level, a S-W particle switches from its initial orientation $\mathbf{m}^{k=I}$ having free energy $G^{k=I}$ calculated from (30) to its final orientation $\mathbf{m}^{k=F}$ with free energy $G^{k=F}$ when the energy difference $G^I - G^F = G^{IF}$ reaches a coercive energy E_c. At the particle level $\xi^I = 1$ or $\xi^F = 1$ and all other volume fractions are zero, the total free energy from (29) is then

$$G = \xi^I G^I + \xi^F G^F - \mathbf{s} \cdot \mathbf{T}, \tag{37}$$

and the second law (23) is

$$-\frac{\partial G}{\partial \xi^I}\dot{\xi}^I - \frac{\partial G}{\partial \xi^F}\dot{\xi}^F = -G^I\dot{\xi}^I - G^F\dot{\xi}^F \geq 0. \tag{38}$$

The criterion for switching from $\mathbf{m}^I$ to $\mathbf{m}^F$ can be implemented by expressing the volume fraction evolution $\dot{\xi}^F = -\dot{\xi}^I$ as a dirac-delta function

$$\dot{\xi}^F = \delta(G^{IF} - E_c). \tag{39}$$

The energy dissipation becomes

$$\begin{aligned} &- G^I\dot{\xi}^I - G^F\dot{\xi}^F = G^I\dot{\xi}^F - G^F\dot{\xi}^F = G^{If}\dot{\xi}^F \\ &= G^{IF}\delta(G^{IF} - E_c) = \begin{cases} E_c, \ G^{IF} = E_c \\ 0, \ else \end{cases}. \end{aligned} \tag{40}$$

Thus there is an instantaneous energy dissipation of E_c when switching occurs. A hysteron for changing field or stress is constructed as follows. For each time step, the orientations $\mathbf{m}^k$ are calculated from (36) and the particle energies G^k from (30). The initial state $k = I$ must be known. The final state $k = F$ is taken as the state $k = M$ which has the globally minimum particle energy G^M. After a step change in the field or stress, the kernel state either stays as $k = I$ or switches to $k = M$ if the energy difference between the two states is greater than the coercive energy. The magnetization and strain are then calculated from (31) and (32) where ξ^k is zero except for $k = I$ or $k = M$ if switching has occurred.

This hysteron can describe the general shape of the magnetization versus field curves in Figures 1(a) and 3(a) as well as the magnetization versus stress curves in Figures 3(b), 1(c) and 1(c). For $\langle 100 \rangle$ oriented, research grade

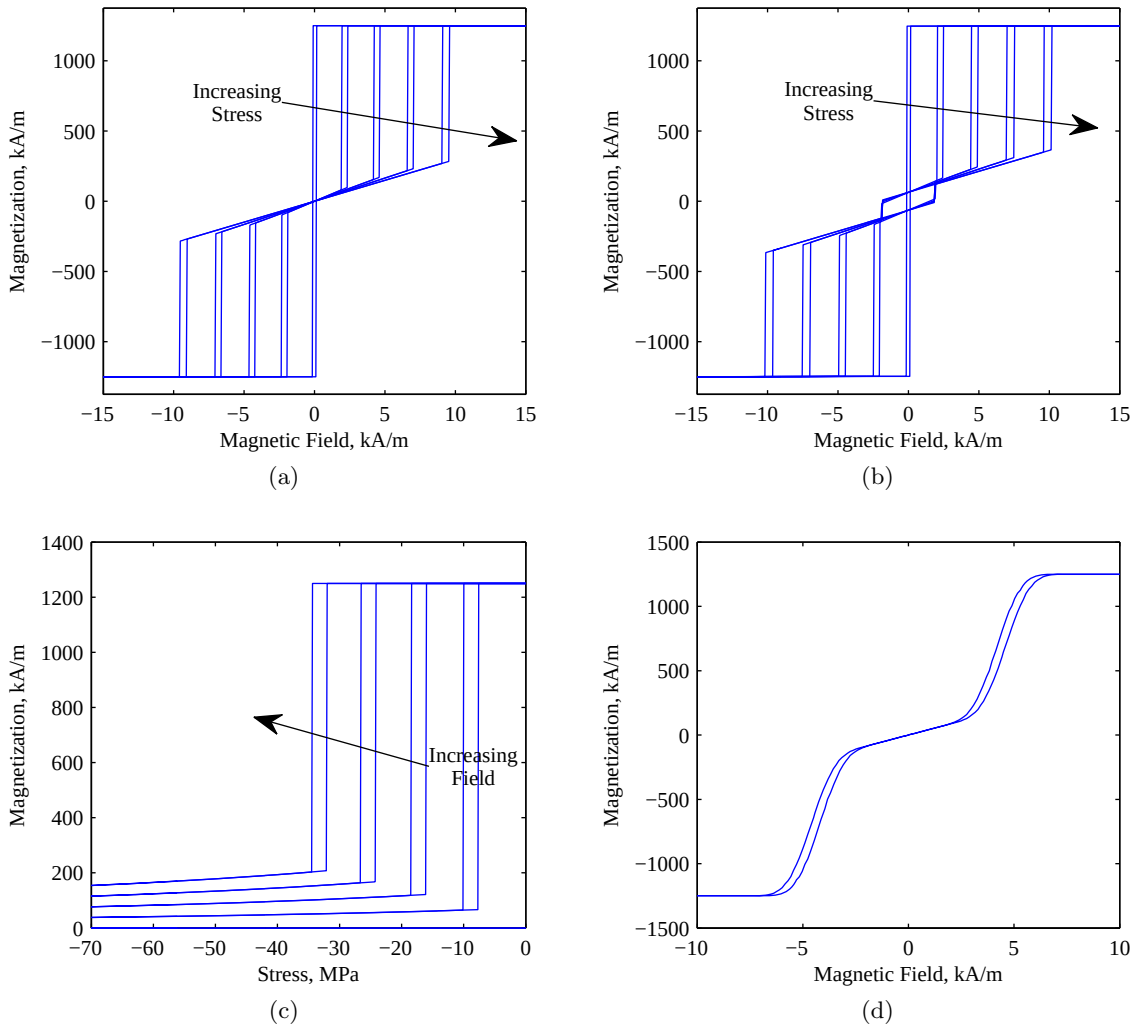

Figure 5. Magnetization versus field hysterons with (a) no misalignment and (b) misalignment, (c) magnetization versus stress hysterons and (d) homogenization of magnetization versus field kernels at constant stress.

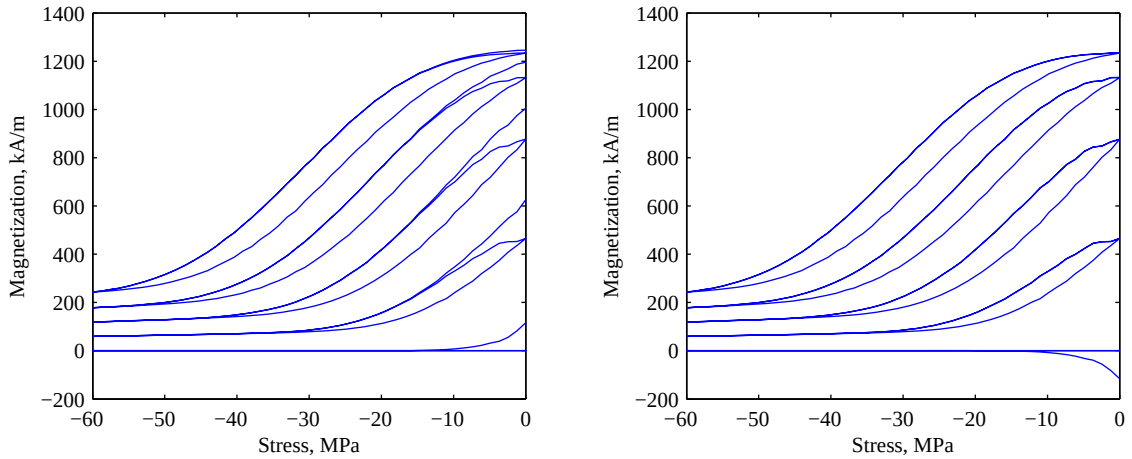

Figure 6. Simulated magnetization versus stress loops with bias field applied (a) after positive saturation and (b) after negative saturation.

material a $\langle 100 \rangle$ orientation is aligned with the rod axis which is the direction of field and stress. The stress dependence of the hysteretic burst regions in 3(a) can be understood from the hysterons in Figure 5(a). The low field linear region is due to rotation of the $\langle 100 \rangle$ domains perpendicular to the field direction. The burst region occurs as domains flip to the $\langle 100 \rangle$ direction aligned with the field. The coercive or dissipation energy E_c causes a delay resulting in hysteresis. With increased stress, higher fields are required to overcome the coercive energy resulting in a shift in the burst region. The additional hysteretic region at low fields for the production grade, field applied major loops results from misalignment. Some of the $\langle 100 \rangle$ directions near the plane perpendicular to the rod axis are closer to the negative rod direction and others to the positive rod direction. Thus hysteretic switching occurs between these directions as the field crosses zero (see Figure 5(b).)

Magnetization versus stress loops in Figures 3(b), 1(c) and 1(c) can be understood from hysterons in Figure 5(c). Stress causes domain switching from the bias field direction or high state to the perpendicular plane or low state. At low stresses, when the material has been saturated positively prior to application of the bias field, all of the hysterons that are double valued will be at the high state. Application of stress moves them to the low state and upon removal of the stress they are still in the low state. This causes causes non-closure of the first loop. Subsequent loops start and end in the low state and hence are closed. When the material is saturated negatively prior to bias field application, the hysterons all start in the low state and hence the first loop is closed also. A departure from this pattern occurs when the bias field is zero. In this case the magnetization begins negative because some hysterons are in the state described by the $\langle 100 \rangle$ orientation in the negative rod direction. Applied stress flips the domain to the perpendicular plane. Further cycles do not result in magnetization change because there is no field causing a preference for either the positive or negative rod directions.

3.3. Stochastic homogenization

Material inclusions and lattice imperfections cause variations in the magnetic field and coercive energy [6]. The macroscopic magnetization and strain can be calculated through stochastic homogenization

$$\bar{\mathbf{M}}(\mathbf{H}, \mathbf{T}) = \int \int \mathbf{M}(\mathbf{H} + \mathbf{H}_I, \mathbf{T}, E_c) \nu(\mathbf{H}_I, E_c) d\mathbf{H}_I dE_c, \tag{41}$$

$$\bar{\mathbf{S}}(\mathbf{H}, \mathbf{T}) = \int \int \mathbf{S}(\mathbf{H} + \mathbf{H}_I, \mathbf{T}, E_c) \nu(\mathbf{H}_I, E_c) d\mathbf{H}_I dE_c. \tag{42}$$

The homogenization procedure (41) is similar to the homogenized energy model of Smith et al. [6] when thermal activation is neglected. Different energy potentials are used for the hysterons and the energy formulation here

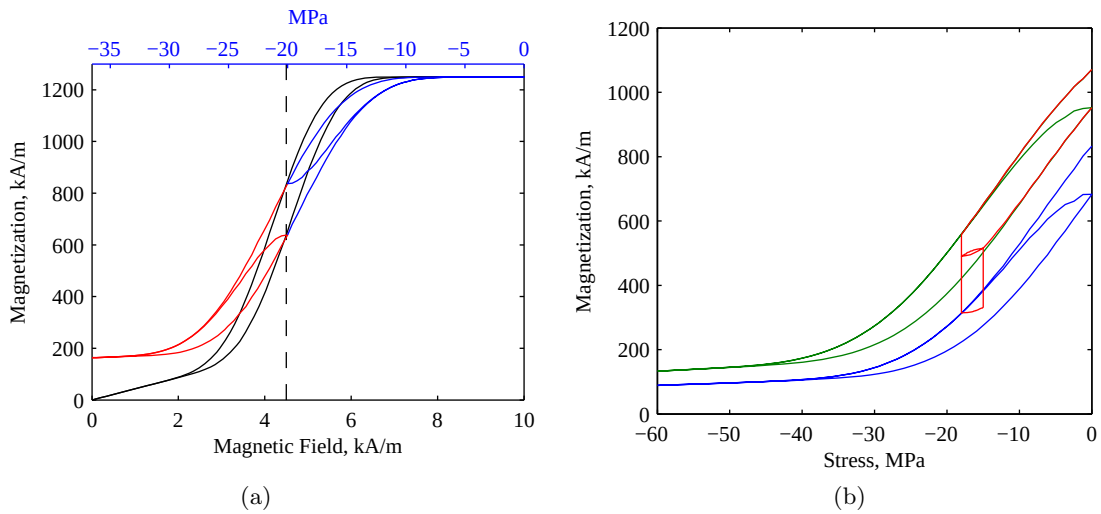

Figure 7. (a) magnetization excursions from the upper and lower hysteresis branches about a bias, cycled three times and (b) minor loops from alternately varying the field and stress about a bias point, cycled times.

is done in 3-D. Additionally, a coercive energy consistent with the second law of thermodynamics was defined rather than a coercive field. This new homogenized energy model has the potential to accurately simulate 3-D and hysteretic constitutive behavior of anisotropic materials. The intent here is to demonstrate that the hysteresis mechanism agrees with properties observed in measurements.

The model is implemented by splitting the integrals into intervals and using 4-point Guass quadrature integration for each interval. Density functions are chosen as Guassian for the interaction field and exponential for the coercive energy, without optimizing for the measurements. Magnetization is thus calculated as the sum of hysterons each with a different interaction field and coercive energy. The result is to smooth the sharp transitions in the hysterons (see Figure 5(d).) Figures 6(b) and 6(a) show simulations of magnetization versus stress loops for the conditions where the material is saturated positively prior to bias field application and negatively prior to bias field application. For the positive saturation case, the first loop is open and subsequent loops are closed. For the negative saturation case, all loops are closed except for the zero field bias case where stress removes the remanent magnetization.

Since the hysterons are stress and field dependent with a delay characterized by a single parameter, the coercive energy, the widths of the hysteretic regions in the magnetization versus field and magnetization versus stress curves are coupled. This is demonstrated in Figure 7(a); when applying a stress about a field and stress bias point starting from the top branch of a major magnetization versus field loop, the magnetization is pushed to the lower branch. Subsequent excursions from a cyclic stress always return to the lower branch. Starting from the lower branch, decreasing the stress followed by returning to the bias stress pushes the magnetization to the upper branch. Further stress cycles always return to the upper branch. This agrees with measurements in Figure 4(a). Biased minor loops obtained from alternately varying the field and stress give shapes similar to experiment and repeated loops do not exhibit accommodation (see Figures 7(b) and 2(b).)

4. CONCLUDING REMARKS

Measurements were presented to characterize the coupled nonlinear and hysteretic magnetization of production and research grade Galfenol due to applied stress and field. It was shown that hysteresis for both applied quantities can be attributed to the same physical mechanism and that major magnetization versus stress loops in compression depend heavily on magnetic history at low stress levels. A remarkable degree of reversibility in the magnetomechanical coupling was demonstrated by generating the same magnetization versus stress hysteresis loop both from a series of constant stress experiments and from a single constant field experiment. Cyclic application of alternately applied field and stress did not result in any noticeable accommodation.

A thermodynamic framework was developed to describe the observed nonlinear and hysteretic behavior. A unified hysteresis mechanism, consistent with the second law of thermodynamics, was developed to account for the coupled magnetic hysteresis due to field and stress application. Stochastic homogenization, similar to Smith's homogenized energy framework [6], was used to incorporate material defects. By choosing appropriate density functions for the interaction and coercive fields, Smith's homogenized energy model accurately simulated steel, nickel, Terfenol-D, as well as ferroelectric materials [7, 9]. For the simulations presented in this work, the densities were chosen a priori as Gaussian for the interaction field and exponential for the coercive energy, without optimizing the standard deviation. Optimizing the densities to minimize error with the measurements and using general density formulations, it is expected that the framework developed here will accurately model the 3D, anisotropic, and hysteretic response of Galfenol and other magnetostrictive materials.

ACKNOWLEDGMENTS

We wish to acknowledge the financial support by the Office of Naval Research, MURI grant #N000140610530. Measurements were performed at the Naval Surface Warfare Centery, Carderock Division as part of the Naval Research Enterprise Internship Program with Marilyn Wun-Fogle and James Restorff as mentors.

REFERENCES

1. A. E. Clark, J. B. Restorff, M. Wun-Fogle, T. A. Lograsso, and D. L. Schlagel, "Magnetostrictive properties of body-centered cubic Fe-Ga and Fe-Ga-Al alloys," *IEEE Trans. Magn.* **36**(5), pp. 3238–3240, 2000.
2. R. A. Kellogg, A. Flatau, A. E. Clark, M. Wun-Fogle, and T. Lograsso, "Quasi-static transduction characterization of Galfenol," *Journal of Intelligent Material Systems and Structures* **16**, pp. 471–479, 2005.
3. M. Wun-Fogle, J. B. Restorff, and A. E. Clark, "Magnetomechanical coupling in stress-annealed Fe-Ga (Galfenol) alloys," *IEEE Transactions on Magnetics* **42**, pp. 3120–3122, October 2006.
4. K. C. Pitman, "The influence of stress on ferromagnetic hysteresis," *IEEE Trans. Magn.* **26**(5), pp. 1978–1980, 1990.
5. D. J. Craik and M. J. Wood, "Magnetization changes induced by stress in a constant applied field ," *Journal of Physics D Applied Physics* **3**, pp. 1009–1016, jul 1970.
6. R. C. Smith, M. J. Dapino, T. R. Braun, and A. P. Mortensen, "A homogenized energy framework for ferromagnetic hysteresis," *IEEE Transactions on Magnetics* **42**(4), pp. 1747–1769, 2005.
7. R. C. Smith and M. J. Dapino, "A homogenized energy model for the direct magnetomechanical effect," *IEEE Transactions on Magnetics* **42**(8), pp. 1944–1957, 2006.
8. C. Kittel, "Physical theory of ferromagnetic domains," *Review of Modern Physics* **21**, pp. 541–583, Oct 1949.
9. R. C. Smith, A. G. Hatch, B. Mukherjee, and S. Liu, "A homogenized energy model for hysteresis in ferroelectric materials: general density formulation," *Journal of Intelligent Material Systems and Structures* **16**, pp. 713–732, 2005.